CBPF-NF-035/82

MOLECULAR ORBITAL STUDY OF IRON PENTACARBONYL AND ITS PHOTOCHEMICAL FRAGMENTS $Fe(CO)_n$

by

D.Guenzburger[1], E.M.B.Saitovitch[1],
M.A. de Paoli[2], and H.Manela[3]

[1]Centro Brasileiro de Pesquisas Físicas - CBPF/CNPq
Rua Xavier Sigaud, 150
22290 - Rio de Janeiro, RJ - BRASIL

[2]Instituto de Química
Universidade Estadual de Campinas
Caixa Postal 1170
13100 - Campinas, SP - BRASIL

[3]Departamento de Física
Pontifícia Universidade Católica
Rua Marquês de São Vicente, 225
22453 - Rio de Janeiro, RJ - BRASIL

MOLECULAR ORBITAL STUDY OF IRON PENTACARBONYL AND ITS PHOTOCHEMICAL FRAGMENTS $Fe(CO)_n$.

Diana Guenzburger, Elisa M.B. Saitovitch,

Centro Brasileiro de Pesquisas Físicas
Rua Xavier Sigaud, 150
22290 Rio de Janeiro, RJ, BRASIL

Marco Aurélio de Paoli,

Instituto de Química
Universidade Estadual de Campinas
Caixa Postal 1170
13100 Campinas, SP, BRASIL

and Henrique Manela

Departamento de Física
Pontificia Universidade Católica
Rua Marques de São Vicente, 225
22453 Rio de Janeiro, RJ, BRASIL

ABSTRACT

Self-consistent Molecular Orbital calculations were performed for $Fe(CO)_5$ and its photofragments $Fe(CO)_n$, $1 \leq n < 5$. The discrete variational method was employed, with the Xα local approximation for the exchange interaction. In the case of $Fe(CO)_5$, photoelectron and optical spectra are analysed, and photochemical behaviour is discussed. The Mössbauer isomer shifts and quadrupole splittings are investigated. In the case of $Fe(CO)_5$ and $Fe(CO)_4$, the values derived for these hyperfine interactions are compared to experimental measurements reported in a polyethylene matrix.

1. INTRODUCTION

The chemical bond in clusters of transition metal atoms and carbonyls is an interesting subject for experimental and theoretical investigations. Among other reasons, there is hope that such systems are good prototypes for situations of carbonyls adsorbed on transition metal surfaces[1]. In this context, there is interest in studying a transition metal atom bound to different numbers of carbonyl ligands.

It is well known that iron pentacarbonyl undergoes photochemical fragmentation[2], in which may be produced species $Fe(CO)_n$, where $5 > n \geq 1$[3]. The solid gas matrix isolation technique has made possible the production by photolysis of fragments $Fe(CO)_n$ and subsequent measurements of spectroscopic properties. In this manner, the infrared spectra of $Fe(CO)_4$ and $Fe(CO)_3$ were measured and analysed[4]-[6], and structural information was derived.

A different manner of obtaining isolated molecules in a solid is absorption in polymer matrixes. This procedure has the advantage that no complicated low-temperature techniques are necessary. In this manner, photochemical reactions of $Fe(CO)_5$ were observed[7]. In our first report[8] was described a study of the photochemical decomposition of $Fe(CO)_5$ sorbed in a film of polyethylene. The fragment $Fe(CO)_4$ was detected, and identified by infra-red spectroscopy. In addition, a study by Mössbauer spectroscopy allowed the measurement of the isomer shift (IS) and quadrupole splitting (ΔEQ) of the tetracarbonyl fragment and parent molecule isolated in the polymer.

The analysis of the available experimental data on the

$Fe(CO)_n$ clusters would certainly be more complete if made together with results obtained with some theoretical model. For this purpose, Molecular Orbital calculations of the Fe carbonyl fragments were performed and the results are described in this second report. The electronic transitions and one-electron levels of $Fe(CO)_5$ are compared to available experimental data on optical spectrum[9] and binding energies[1],[10]. The Mössbauer parameters IS and ΔEQ are calculated for all fragments. For the case of $Fe(CO)_5$ and $Fe(CO)_4$, they are compared to the experimental values obtained[8]; for the smaller clusters, predictions are made. The trends of the calculated values of these parameters are analysed and discussed, with the aid of the description of the electronic structures obtained with the Molecular Orbital calculations.

2. MOLECULAR ORBITAL MODEL

Molecular Orbital calculations of transition metal compounds have been performed in a great number of cases with the use of the local density approximation for the exchange interaction, known as Xα approximation. Successful interpretation of spectroscopic and other molecular properties has been achieved, with considerably smaller computational effort than the full "ab-initio" Molecular Orbital (MO) method. The Xα exchange approximation is usually employed in the Multiple Scattering (MSXα)[11] method, where a "muffin-tin" model potential is used to simulate the molecular potential, and in the discrete variational method (DVM)[12], where the molecular orbitals are expanded in a basis of numerical atomic functions and the variational scheme

leads to secular equations formally equal to those obtained in the Hartree-Fock-Roothaan MO method, but where the matrix elements are calculated numerically.

The calculations reported here were performed with the DVM method. We shall not describe this model in detail, but refer the reader to the original literature[12]. The discrete variational method leads to the secular equations:

$$(\underset{\sim}{H} - E\,\underset{\sim}{S})\,\underset{\sim}{C} = 0 \qquad (1)$$

where the matrix elements are numerical integrals. The integrations are performed in three dimensions with the statistical Diophantine method. The one-electron Hamiltonian is expressed as (in Hartrees):

$$H = -\frac{1}{2}\nabla^2 + V_{coul} + V_{x\alpha} \qquad (2)$$

where $V_{x\alpha}$ is the Xα exchange potential[13]

$$V_{x\alpha\uparrow}(\vec{r}) = -3\alpha[(3/4\Pi)\rho_{\uparrow}(\vec{r})]^{1/3} \qquad (3)$$

where $\rho_{\uparrow}(\vec{r})$ is the electronic density of spin up electrons at point $\vec{r}$, and a similar expression is given for spin down. In the present calculations the value $\alpha = 2/3$ was employed[13]. The Coulomb potential V_{coul} has an approximate form, in which a superposition of spherical charge densities around each atomic nucleus is used to generate the molecular potential[12]. The electric field gradient (EFG) matrix elements in the evaluation

of ΔEQ are calculated in full over the molecular wave functions, using special numerical integration schemes[14].

All electrons are taken into account in the MO calculations. A Mulliken-type population analysis is performed(15), and iterations are made until the populations are self-consistent. The atomic basis functions, in the case of Fe, are extended to include virtual orbitals; to obtain these orbitals as bounded, a spherical potential well is added to the atomic potential.

3. ELECTRONIC STRUCTURE AND PROPERTIES OF $Fe(CO)_5$

We shall begin the description of the MO calculations results by discussing in some detail the parent compound of the fragments, iron pentacarbonyl. This compound, a yellow liquid soluble in organic solvents, undergoes photochemical decomposition, the resulting fragment $Fe(CO)_4$ having been detected in solid gas matrixes[4][5] and polyethylene[8], whereas the fragment $Fe(CO)_3$ was identified in solid gas matrixes after prolonged UV photolysis[6]. One-photon absorption of gaseous $Fe(CO)_5$ irradiated with a pulsed laser source at different UV wavelengths resulted in the obtention of all fragments $Fe(CO)_n$, $1 \leq n \leq 4$, with yields that varied with the wavelength of the radiation[3].

$Fe(CO)_5$ is known to have a D_{3h} structure in the ground state[9] (see Fig. 1). The interatomic distances considered here were the same as in reference [9], namely Fe-C(equatorial) = 1.79 Å, Fe-C (axial) = 1.81 Å, C - O(eq.) = 1.13 Å and C-O(ax) = 1.11 Å.

The one-electron eigenvalues obtained for $Fe(CO)_5$ are shown in Fig.2 and Table 1. In Fig.2 the energy levels scheme is compared to the valence photoelectron spectrum[10b], and it is seen

that the orbitals scheme is compatible with the experimental measurements, the two upper 10e' and 3e" orbitals, of primarily Fe(3d) nature, being quite separate from the ligand levels, and originating the two lower energy peaks. A more quantitative evaluation of binding energies require a transition state calculation[13] for each level; here, we are satisfied that the overall agreement guarantees a reasonable description of the electronic structure. A more accurate and detailed study of the ionization energies of $Fe(CO)_5$ with the DVM method has been reported[16].

In Table 1 is given the approximate charge distribution of the valence orbitals of $Fe(CO)_5$, in terms of a Mulliken[15] population analysis. The occupied valence orbitals, except for the highest-energy 3e"(Fe(3d)) and 10e'(Fe(3d) and (4p)), are localized almost entirely on the carbonyls. Only the $11a_1'$ orbital displays significant Fe(3d) character. Table 2 gives the population analysis of $Fe(CO)_5$. An almost complete depletion of the Fe(4s) orbital has taken place, whereas the 4p has a significant occupation.

The rather striking localization of the bonding valence orbitals on the ligands has lead us to explore the possibility of a bonding mechanism in which a metal $\rightleftarrows$ ligand charge transfer would not play the major role, as is believed to happen in most transition metal complexes. The result of this investigation is depicted in Fig.2. There are shown, from left to right, the self-consistent orbital energies of CO, of the group of five carbonyl ligands arranged as in the complex $((CO)_5\text{-}D_{3h})$, and of the same $(CO)_5$ group, but this time in the presence of the

charge distribution of the Fe atom ($(CO)_5$ + Fe). In this last case, the Fe atom acts as an attractive potential, but does not take part in the variational calculation.

A comparison with the energy levels scheme of $Fe(CO)_5$ shows that indeed the "band" of valence levels due to the $(CO)_5$ group is shifted down by the presence of the Fe charge cloud, presenting a structure similar to that obtained for the actual $Fe(CO)_5$ complex. The only outstanding exception is the lowest $7a_1'$ level of this group, which in the variational calculation of $Fe(CO)_5$ ($10a_1'$) is shifted upwards, probably through orthogonality effects.

This result suggests that the simple description of the $Fe(CO)_5$ molecule as a $(CO)_5$ group clustered together by the attractive potential of the Fe atom, might be an approximatly appropriate model to account, at least partially, for the chemical bond in this complex. It seems worth while to test the validity of this model further on other transition metal carbonyls, and this work is now in progress[17].

We now turn our attention to the electronic transitions of $Fe(CO)_5$. Both differences between vacant and occupied eigenvalues ($\varepsilon_j - \varepsilon_i$) and results of transition state calculations[13] are displayed in Table 3, and compared with the experimental values of the electronic spectrum[9]. All transitions, except those marked (f) in Table 3, are dipole-allowed. Again, the overall agreement found is good. Some of the transitions associated to the band at 35.5 kcm^{-1} are to vacant orbitals of substantial Fe(3d) character (see Table 1). The final states of the excitation from the $^1A_1$ closed-shell ground state are given on the

left column of Table 3.

To end this section, we discuss one of the most interesting aspects of $Fe(CO)_5$ chemistry, namely its photochemical fragmentation. Since the first step in this process is the absorption of UV radiation and consequent transition to some excited state, some knowledge of the electronic structure of low-lying excited states might through light on the decomposition mechanisms.

First, we notice (Table 4) that in the ground state of $Fe(CO)_5$, the negative charge on each equatorial carbonyl is slightly larger than that on each axial carbonyl. One may thus assume that such difference in equatorial-axial charge distribution is important for the stability of the molecule, and proceed by searching low-energy excited states in which this situation is changed, thus leading to instability. Self-consistent calculations were performed for the excited states resulting from the allowed transitions indicated in Table 4, assuming a D_{3h} symmetry for the excited states (Frank-Condon principle). These calculations were done in the spin-polarized approximation, which gives a better description of the excited states since they have open-shell configurations. In a spin-polarized calculation, the molecular orbitals of electrons with opposite spins are allowed to have different spacial extents. Only spin-allowed transitions were considered.

Examination of the charges obtained on the axial and equatorial carbonyls reveals that some transitions, more specifically the two lower-energy transitions $10e' \rightarrow 14a_1'$ and $10e' \rightarrow 11e'$, result in excited states in which negative charge is transferred to the axial carbonyls, compared to the ground state. On the contrary, the higher-energy transitions $3e'' \rightarrow 9a_2''$ and $3e'' \rightarrow 12e'$ give

excited states in which more charge still is transferred from the axial to the equatorial carbonyls.

The experimental yields of photofragments of $Fe(CO)_5$ in the gaseous state obtained by Yardley et al.[3] are reproduced in Table 5. It is seen that higher energy radiation produces preferebly the fragment $Fe(CO)_2$, whereas the fraction of $Fe(CO)_3$ and $Fe(CO)_4$ produced increases when the energy of the radiation is lowered. A simple model to explain these results can be devised with the numbers on Table 4. In fact, one may immagine that transitions in which charge is transferred to the equatorial carbonyls might result in the loss of these three equatorial ligands, producing $Fe(CO)_2$. Reversely, accumulation of charge on the axial ligands might produce $Fe(CO)_3$ and $Fe(CO)_4$, by loss of two or one CO groups.

This is a very simple hypothesis of concerted mechanisms of production of photofragments in the gas phase, which certainly needs more detailed theoretical and experimental investigation. It must be mentioned that Yardley et al.[3] favour a sequential mechanism of fragmentation, in which one carbonyl would be lost in each step, to produce a smaller fragment.

4. ELECTRONIC STRUCTURE OF THE $Fe(CO)_n$ FRAGMENTS

We now turn our attention to some general aspects and trends in the electronic properties of the $Fe(CO)_n$ clusters, the structures of which are shown in Fig. 1. We have assumed for the Fe - C and C - O interatomic distances, averages over the equatorial and axial values of $Fe(CO)_5$.

The $Fe(CO)_4$ fragment was found to have a C_{2v} structure,

with angles 145^{o} and 120^{o}, as in Fig.1, from matrix isolation studies of infrared spectroscopy [5]. The temperature dependence of the magnetic circular dichroism spectrum in an Ar matrix shows that the molecule is paramagnetic [18]. The $Fe(CO)_3$ cluster has had its C_{3v} structure (depicted in Fig.1) determined also by I.R. spectroscopy in low-temperature matrixes, with the angle between two carbonyls found to be $\sim 110^{o}$ [6]. As no experimental determination of the angle between the carbonyls is available for $Fe(CO)_2$, we have explored both the 180^{o} angle ($D_{\infty h}$), and a C_{2v} symmetry with the carbonyls angle equal to 144^{o}. Finally, the FeCO fragment was considered linear.

In Fig. 3 are presented the orbital energy schemes for the fragments $Fe(CO)_n$, calculated in the spin-restricted approximation. The energy levels for atomic Fe, C and O are also given, as well as those of the CO ligand. The smallest fragment FeCO already shows an inversion of the orbitals derived from the 1π and 5σ orbitals of CO. This feature has been also observed in Multiple Scattering $X\alpha$ calculations of $Ni(CO)_n$ fragments [19]. In the higher fragments levels derived from the 1π and 5σ orbitals of CO cluster very closely together. This is compatible with one of the characteristics of transition metal carbonyls photoelectron spectra, which is the non-resolution of the carbonyl 1π and 5σ - derived levels [1].

Some general trends may be noticed in Fig. 3. Both the highest occupied Fe(3d) - derived levels, as well as the band of ligand-derived levels, are shifted to lower energies, as the number of carbonyl groups increases. The Fe(3d) lev-

els are the 1δ, 11σ and 4π in FeCO, $1\delta_g$, $9\sigma_g$ and $2\Pi_g$ in $Fe(CO)_2$, 11e, $12a_1$ and 10e in $Fe(CO)_3$, $19a_1$, $10b_1$, $10b_2$, $18a_1$ and $3a_2$ in $Fe(CO)_4$, and 10e' and 3e" in $Fe(CO)_5$. We also notice that, as the number of carbonyls increases, the Fe(3d) orbitals stabilize more than the band of ligand orbitals, so that the energy difference between these two groups of levels decreases. This increasing stabilization of the Fe(3d) antibonding orbitals also causes an increased energy difference between these levels and the first unnoccupied set of levels. These features should be observed in measurements of ionization energies and electronic spectra.

The energy levels for the spin-polarized calculations are shown in Fig. 4, in which only the Fe(3d)-derived orbitals are drawn in detail. From these calculations, the ground state configurations obtained by simply following the "aufbau" principle, in which orbitals of lower energy are filled first, are exactly those shown in Fig. 3. The spin-polarized calculation of $Fe(CO)_4$ does indeed predict a paramagnetic configuration ($3a_2^2\ 18a_1^2\ 10b_2^2\ 10b_1^1\uparrow 19a_1^1\uparrow$), but the difference between the $19a_1\uparrow$ and $10b_1\downarrow$ level energies is very small, so that, solely on the basis of these calculations, one could not definitly rule out the possibility of a diamagnetic ground state ($3a_2^2\ 18a_1^2\ 10b_2^2\ 10b_1^2$). However, the paramagnetic ground state seems established from experimental measurements[18], as mentioned before.

Another feature to be mentioned about the spin-polarized calculations is that the splitting of the Fe(3d) levels of opposite spins caused by the exchange polarization (there are two unpaired electrons in all clusters, except in closed-shell $Fe(CO)_5$), increases for the smaller fragments.

Complementary information to that given in Figs. 3 and 4 may be found in Table 2, where the Fe orbitals populations and total charges on Fe, C and O are given. It is seen that all fragments have larger Fe(3d) populations that the Fe free atom. The Fe(4s) increases gradually as CO groups are removed. The opposite trend is observed for the Fe(4p). On the whole, it may be concluded that, according to the present calculations, the smaller clusters have configurations that resemble more closely that of the Fe atom.

The charge transfer Fe → carbonyls is small, resulting in a small positive charge on Fe. We also give in Table 2 what we denominated "effective number of unpaired electrons" on Fe, and which is simply the difference between the total spin up and spin down populations of that atom. The increase of this number with the decrease of the number of carbonyls is compatible with the trend, shown in Fig. 4, of the Fe(3d) levels splittings.

5. MÖSSBAUER ISOMER SHIFTS AND QUADRUPOLE SPLITTINGS OF $Fe(CO)_n$ CLUSTERS

As mentioned in the Introduction, the development of photofragmentation techniques of $Fe(CO)_5$ isolated in polymer matrixes has allowed the measurement at room temperature of the Mössbauer isomer shift IS and quadrupole splitting ΔEQ of $Fe(CO)_4$. We have thus investigated these hyperfine interactions in all the $Fe(CO)_n$ clusters, making use of the molecular orbitals obtained. The IS is defined as [20]

$$IS = \frac{2\pi}{3} Ze^2 S'(Z)\, \Delta\langle r^2\rangle \left[\sum_i n_i \left|\psi_i(0)\right|^2_A - \sum_j n_j \left|\psi_j(0)\right|^2_S \right]$$

or (4)

$$IS = \alpha \left[\sum_i n_i \left|\psi_i(0)\right|^2_A - \sum_j n_j \left|\psi_j(0)\right|^2_S \right]$$

where A and S refer to absorber and source, $\Delta\langle r^2\rangle$ is the difference in the mean square nuclear radius in the excited and ground states in the Mössbauer nuclear transition, $S'(Z)$ a factor to correct for relativistic effects, and the summations are over the molecular orbitals ψ_i occupied by n_i electrons. Only s-type functions have values of $|\psi_i(0)|$ that are different from zero.

The quadrupole splitting ΔEQ[20] of the nuclear level of spin $I = 3/2$ of ^{57}Fe, produced by the interaction between the nuclear quadrupole moment Q and the electric field gradient of exterior charges, is given by:

$$\Delta EQ = \frac{eQ}{2} V_{zz} \left(1 + \frac{\eta^2}{3}\right)^{1/2}, \qquad \text{with} \quad \eta = \frac{V_{xx} - V_{yy}}{V_{zz}}$$

$$\text{where} \qquad V_{k\ell} = \sum_i Z_i \frac{(3x_{ik}\, x_{i\ell} - \delta_{k\ell}\, r_i^2)}{r_i^5} \tag{5}$$

are the components of the electric field gradient tensor for the nucleii surrounding the Fe atom. The electronic contributions to the field gradient, in the Molecular Orbital approximation, are given by [14][20]:

$$V_{zz} = -e \sum_i n_i \langle \psi_1 \left| \frac{3\cos^2\theta - 1}{r^3} \right| \psi_i \rangle$$

$$\frac{V_{xx} - V_{yy}}{e} = \sum_i n_i \langle \psi_i \left| \frac{3\mathrm{sen}^2\theta \cos 2\phi}{r^3} \right| \psi_i \rangle \qquad (6)$$

In Table 6 we show the values, calculated in the spin-polarized approximation, of the electron densities at the Fe nucleus ($n_i|\psi_i(0)|^2$) for the Fe(3s) and valence orbitals of the carbonyl fragments. Deeper core orbitals were not considered because the numerical statistical integration does not allow sufficient accuracy for the determination of very small differences between these large numbers. However, these differences may be considered negligible for the present purpose.

Certain trends in the values obtained may be observed, and related to electronic properties. The total (Fe(3s) + valence) electron density at the origin has very similar values for $Fe(CO)_5$ and its fragments, and so similar isomer shifts are predicted. However, one may notice that, as the number of carbonyls decreases, a small decrease in the total electron density is observed; for the smaller fragments $Fe(CO)_2$ and $Fe(CO)$, this trend is reversed. This is explained as follows: in $Fe(CO)_5$, a large valence contribution is calculated. This is not due to a large Fe(4s) population, since this is quite negligible (see Table 2), but to participation of the Fe(3s) orbitals of the basis in the valence molecular orbitals, which may be viewed as a "contraction" (for example, in orbital $10a_1'$ of $Fe(CO)_5$). This "contraction" is decreased slightly in $Fe(CO)_4$, resulting in a slightly smaller density. As the number of CO ligands decreases further, an increase in Fe(4s) populations occurs, and this compensates for the smaller "contraction" of valence orbitals.

For example, the orbitals 11σ of FeCO and $9\sigma_g$ of $Fe(CO)_2$ ($D_{\infty h}$) have large 4s components.

In Table 7 are given the calculated IS values; they were obtained by fitting the experimental value of $Fe(CO)_5$ in the polyethylene matrix[8], and by using $\alpha = -0.29$ in Eq.(4). This value of α was derived theoretically from a study of several Fe compounds with the MSXα method[21]. The theoretical value for $Fe(CO)_4$ may be compared to the experimental value (0.124) in the polimer matrix. Although the trend is correct, the numerical agreement is not good, which shows that, for such small differences in IS values, one cannot expect great accuracy with the present approximations.

Finally, the results for the spin-polarized calculations of the quadrupole splittings are given in Table 8. The deep core orbitals of Fe (1s, 2s and 2p) were neglected. Again, the calculated value for $Fe(CO)_5$ was fitted to experiment; this value corresponds to $Q = 0.158b$ in Eq.(5), which is very close to the value $Q = 0.15b$ recently derived from theoretical calculations[22]. The value obtained here for $Fe(CO)_4$ agrees well with the experimental number. The sign of the electric field gradient, which could not be obtained experimentally, is predicted to be positive, as in $Fe(CO)_5$.

The negative values calculated for ΔEQ of FeCO and $Fe(CO)_2$ are surprisingly large for Fe compounds. Although these results might motivate an experimental investigation, they however must be viewed with caution. In Table 9 are shown, for these two fragments, the one-center contributions to V_{zz} due to the Fe(3d) orbitals. It is seen that the total field gradi

ent depends on a delicate balance of large positive and negative terms. A different ground-state configuration than that predicted here might alter the calculated values of ΔEQ to a large extent.

6. CONCLUSIONS

The Discrete Variational-Xα Molecular Orbital calculations performed for Fe carbonyl clusters have given insight into several aspects of the electronic structure, both of the parent compound $Fe(CO)_5$ and of the smaller fragments. We have discussed the Molecular Orbital energies and related properties of iron pentacarbonyl, as well as aspects of its photochemical behaviour. Trends in the electronic structures and bonding features were obtained for all fragments. As for the Mössbauer isomer shifts and quadrupole splittings, the results obtained may be considered reliable as far as trends are concerned, and allow to relate these hyperfine interactions to characteristics of the chemical bonds. However, accurate numerical values cannot be expected, for such small effects, at this level of approximation.

REFERENCES

[1] E.W. Plummer, W.R. Salaneck, and J.S. Miller, Phys. Rev.B, 18, 1673(1978).

[2] M. Wrighton, Chem. Revs., 74, 401(1974).

[3] J.T. Yardley, B. Gitlin, G. Nathanson, and A.M. Rosan, J. Chem. Phys., 74, 370(1981).

[4] M. Poliakoff, and J.J. Turner, J. Chem. Soc. (Dalton Trans.), 1973, 1351.

[5] M. Poliakoff, and J.J. Turner, J. Chem. Soc. (Dalton Trans.), 1974, 2276.

[6] M. Poliakoff, J. Chem. Soc. (Dalton Trans.), 1974, 210.

[7] M.A. de Paoli, S.M. Oliveira, and F. Galembeck, J. Organometall. Chem., 193, 105(1980).

[8] S.M. Oliveira, M.A. de Paoli, E. M. B. Saitovitch, and D. Guenzburger, this journal.

[9] M. Dartiguenave, Y. Dartiguenave, and H.B. Gray, Bull. Soc. Chim. France, 12, 4223(1969).

[10] (a) D.R. Lloyd, and E.W. Schlag, Inorg. Chem., 8, 2544(1969); (b) J.L. Hubbard, and D.L. Lichtenberger, J. Chem. Phys., 75, 2560(1981).

[11] See, for example, K.H. Johnson, Advan. Quant. Chem., 7, 143(1973).

[12] D.E. Ellis, Int. J. Quant. Chem., S2, 35(1968); D.E. Ellis, and G.S. Painter, Phys. Rev. B, 2, 2887(1970); A. Rosén, D. E. Ellis, H. Adachi, and F.W. Averill, J. Chem. Phys., 85, 3629(1976).

[13] J.C. Slater, "The Self-Consistent Field for Molecules and Solids", vol.4 of "Quantum Theory of Molecules and Solids",

McGraw-Hill, N. York (1974).

[14] D. Guenzburger, and D.E. Ellis, Phys. Rev. B, 22, 4203(1980).

[15] C. Umrigar, and D.E. Ellis, Phys. Rev. B., 21, 852(1980).

[16] E.J. Baerends, and P. Ros, Mol. Phys., 30, 1735(1975);

[17] D. Guenzburger, unpublished.

[18] T.J. Barton, R. Grinter, and A.J. Thomson, J. Chem. Soc. Chem. Comm., 1977, 841.

[19] I.A. Howard, G.W. Pratt, and K.H. Johnson, J. Chem. Phys., 74, 3415(1981).

[20] See, for example: G.M. Bancroft, "Mössbauer Spectroscopy", McGraw-Hill, London(1973); N.N. Greenwood, and T.C. Gibb, "Mössbauer Spectroscopy", Chapman and Hall, London(1971).

[21] D. Guenzburger, D.M.S. Esquivel, and J. Danon, Phys. Rev.B, 18, 4561(1978).

[22] S.N. Ray, and T.P. Das, Phys. Rev. B, 16, 4794(1977).

TABLE CAPTIONS

Table 1 - Molecular orbitals energies and charge distributions for Iron Pentacarbonyl.

Table 2 - Fe orbitals populations, charges, and effective number of unpaired electrons on Fe for $Fe(CO)_n$, $1 \leq n \leq 5$.

Table 3 - Theoretical and experimental electronic transitions of $Fe(CO)_5$.
(a) From Reference (9).

Table 4 - Charge distribution on equatorial and axial carbonyls of $Fe(CO)_5$ in ground and excited states.

Table 5 - Relative yields of photofragments obtained by laser irradiation of gaseous $Fe(CO)_5$. From Reference [3].

Table 6 - Contributions $(n_i|\psi_i(0)|^2)$ of molecular orbitals ψ_i to the electron density at the Fe nucleus in Fe carbonyl clusters.

Table 7 - Experimental (Reference [8]) and calculated values of isomer shifts of $Fe(CO)_n$ clusters.

Table 8 - Experimental (Reference [8]) and calculated values of quadrupole splittings of $Fe(CO)_n$ clusters.

Table 9 - Individual orbital values of the one-center contributions to the field gradient V_{zz} of FeCO and $Fe(CO)_2$.

FIGURE CAPTIONS

Figure 1 - Structure of Iron Pentacarbonyl and $Fe(CO)_n$ fragments.

Figure 2 - Orbital energy levels schemes for CO, $(CO)_5$, $(CO)_5$ in the presence of a Fe potential, and $Fe(CO)_5$.
(a) Photoelectron spectrum from Reference (10b).

Figure 3 - Orbital energy levels for CO and for $Fe(CO)_n$, $1 \leq n \leq 5$, obtained with spin-restricted calculations.

Figure 4 - Orbital energy levels for $Fe(CO)_n$, $1 \leq n \leq 5$, obtained with spin-polarized calculations.

TABLE 1

Orbital	Energy (in eV)	Charge Distribution (in % of one electron)
$10a_1'$	-19.42	23 $C_{ax}(2s)$,20 $C_{ax}(2p)$,25 $C_{eq}(2s)$, 21 $C_{eq}(2p)$
6e'	-17.15	8 Fe(3d),49 $C_{eq}(2s)$,23 $C_{eq}(2p)$,13 $O_{eq}(2s)$
$11a_1'$	-16.78	26 Fe(3d),19 $C_{ax}(2s)$,10 $C_{ax}(2p)$,20 $C_{eq}(2s)$,10 $C_{eq}(2p)$, 5 $O_{ax}(2s)$,6 $O_{eq}(2s)$
$6a_2''$	-16.76	50 $C_{ax}(2s)$,20 $C_{ax}(2p)$,18 $O_{ax}(2s)$,5 $O_{ax}(2p)$
1e"	-14.59	5 Fe(3d),35 $C_{ax}(2p)$,22 $C_{eq}(2p)$,25 $O_{ax}(2p)$,14 $O_{eq}(2p)$
$12a_1'$	-14.38	7 $C_{ax}(2p)$,23 $O_{ax}(2s)$,60 $O_{ax}(2p)$
$13a_1'$	-14.21	6 Fe(3d),7 $C_{eq}(2p)$,23 $O_{eq}(2s)$,56 $O_{eq}(2p)$
7e'	-14.15	9 $C_{eq}(2p)$,23 $O_{eq}(2s)$,54 $O_{eq}(2p)$
$7a_2''$	-14.02	9 $C_{ax}(2p)$,14 $C_{eq}(2p)$,18 $O_{ax}(2s)$,46 $O_{ax}(2p)$,10 $O_{eq}(2p)$
8e'	-13.99	9 $C_{ax}(2p)$,36 $C_{eq}(2p)$,13 $O_{ax}(2p)$,34 $O_{eq}(2p)$
9e'	-13.43	17 $C_{ax}(2p)$,13 $C_{eq}(2p)$,45 $O_{ax}(2p)$,17 $O_{eq}(2p)$
$1a_2'$	-13.32	35 $C_{eq}(2p)$,65 $O_{eq}(2p)$
2e"	-13.22	11 $C_{ax}(2p)$,19 $C_{eq}(2p)$,29 $O_{ax}(2p)$,41 $O_{eq}(2p)$
$8a_2''$	-13.08	9 Fe(4p),10 $C_{ax}(2s)$,6 $C_{ax}(2p)$,13 $C_{eq}(2p)$,6 $O_{ax}(2p)$, 52 O_{eq}
3e"	- 9.83	70 Fe(3d),14 $O_{ax}(2p)$,13 $O_{eq}(2p)$
$10e'^{(4)}$	- 8.87	15 Fe(4p),50 Fe(3d),7 $C_{eq}(2p)$,18 $O_{eq}(2p)$
$9a_2''^{(o)}$	- 4.65	8 $C_{ax}(2s)$,44 $C_{eq}(2p)$,43 $O_{eq}(2p)$
$2a_2'$	- 4.38	57 $C_{eq}(2p)$,43 $O_{eq}(2p)$
$14a_1'$	- 4.37	48 Fe(3d),18 $C_{ax}(2s)$,10 $C_{ax}(2p)$,7 $C_{eq}(2s)$,5 $C_{eq}(2p)$
11e'	- 4.37	6 Fe(3d),40 $C_{ax}(2p)$,8 $C_{eq}(2s)$,42 $O_{ax}(2p)$
4e"	- 4.34	23 Fe(3d),14 $C_{ax}(2p)$,32 $C_{eq}(2p)$,11 $O_{ax}(2p)$,21 $O_{eq}(2p)$
12e'	- 3.84	22 Fe(3d),6 $C_{eq}(2s)$,37 $C_{eq}(2p)$,30 $O_{eq}(2p)$
5 e"	- 3.30	32 $C_{ax}(2p)$,24 $C_{eq}(2p)$,26 $O_{ax}(2p)$,17 $O_{eq}(2p)$

TABLE 2

	CO	FeCO	$Fe(CO)_2$ $D_{\infty h}$	$Fe(CO)_2$ C_{2V}	$Fe(CO)_3$	$Fe(CO)_4$	$Fe(CO)_5$
Fe populations: 3s	-	1.98	1.97	1.97	1.96	1.94	1.93
3p	-	5.99	5.98	5.98	5.97	5.95	5.95
3d	-	6.44	6.49	6.54	6.60	6.61	6.65
4s	-	1.02	0.86	0.54	0.12	0.07	0.01
4p	-	0.08	0.08	0.21	0.39	0.46	0.53
4d	-	0.07	0.13	0.13	0.18	0.21	0.26
5s	-	0.02	0.03	0.02	0.02	0.03	0.04
5p	-	0.02	0.03	0.04	0.07	0.09	0.11
Charges: Fe	-	0.37	0.43	0.57	0.70	0.64	0.53
C	+0.23	-0.17	-0.08	-0.15	-0.12	-0.06	-0.02
O	-0.23	-0.20	-0.14	-0.14	-0.12	-0.09	-0.08
Effective number of unpaired electrons on Fe	-	2.49	2.46	2.47	1.90	1.54	-

TABLE 3

Final State	One - electron transition	Calculated energies (in kcm^{-1})		Experimental[a] (300°K)	
		$\varepsilon_j - \varepsilon_i$	transition state calculation	Energy (kcm^{-1})	ε
E"	$10e' \rightarrow 9a_2''$ (f)	33.9	35.0		
E'	$10e' \rightarrow 2a_2'$	36.2	37.2		
E'	$10e' \rightarrow 14a_1'$	36.3	36.4	35.5	3,800
E'	$10e' \rightarrow 11e'$	36.3	37.2		
A_2''	$10e' \rightarrow 4e''$	36.5	37.0		
E'	$10e' \rightarrow 12e'$	40.6	40.9		
E'	$3e'' \rightarrow 9a_2''$	41.6	43.4		
E"	$3e'' \rightarrow 2a_2'$(f)	43.9	45.6	41.5	10,200
E"	$3e'' \rightarrow 14a_1'$(f)	44.0	43.9		
A_2''	$3e'' \rightarrow 11e'$	44.0	45.4		
E'	$3e'' \rightarrow 4e''$	44.3	45.0		
A_2''	$10e' \rightarrow 5e''$	44.9	46.0		
A_2''	$3e'' \rightarrow 12e'$	48.3	48.9	50.0	37,000
E'	$3e'' \rightarrow 5e''$	52.7	54.3		

TABLE 4

	Energy of Transition (in kcm^{-1})	Final State and Polarization	Charge of axial CO	Charge of Equatorial CO
Ground State	-	-	-0.075	-0.126
$10e' \rightarrow 14a_1'$	36.4	E'(x,y)	-0.117	-0.104
$10e' \rightarrow 11e'$	37.2	E'(x,y)	-0.171	-0.092
$3e'' \rightarrow 9a_2''$	43.4	E'(x,y)	-0.003	-0.197
$3e'' \rightarrow 12e'$	48.9	A_2'' (z)	-0.013	-0.188

TABLE 5

	Energy of laser radiation (in kcm^{-1})		
	28.4	40.3	51.8
FeCO	-	-	0.012
$Fe(CO)_2$	0.31	0.55	0.81
$Fe(CO)_3$	0.46	0.35	0.09
$Fe(CO)_4$	0.23	0.10	0.09

TABLE 6

FeCO $C_{\infty v}$		$Fe(CO)_2$ $D_{\infty h}$		$Fe(CO)_2$ C_{2v}		$Fe(CO)_3$ C_{3v}		$Fe(CO)_4$ C_{2v}		$Fe(CO)_5$ D_{3h}	
6σ	140.940	$5\sigma_g$	141.010	$6a_1$	140.972	$6a_1$	140.575	$8a_1$	140.407	$7a_1'$	140.456
7σ	0.	$6\sigma_g$	0.	$7a_1$	0.011	$7a_1$	0.017	$9a_1$	0.006	$8a_1'$	0.
8σ	0.	$7\sigma_g$	2.745	$8a_1$	0.	$8a_1$	0.001	$10a_1$	0.	$9a_1'$	0.003
9σ	1.586	$8\sigma_g$	0.748	$9a_1$	2.862	$9a_1$	4.362	$11a_1$	0.001	$10a_1'$	6.065
10σ	0.751	$9\sigma_g^{(2)}$	3.664	$10a_1$	0.847	$10a_1$	1.016	$12a_1$	5.312	$11a_1'$	0.113
$11\sigma^{(2)}$	3.981		148.17	$11a_1$	0.019	$11a_1$	0.005	$13a_1$	0.029	$12a_1'$	0.390
	147.26			$12a_1^{(2)}$	1.863	$12a_1^{(2)}$	0.437	$14a_1$	0.509	$13a_1'^{(2)}$	0.422
				$13a_{1\uparrow}^{(1)}$	0.415		146.41	$15a_1$	0.371		147.45
					146.99			$16a_1$	0.036		
								$17a_1$	0.054		
								$18a_1^{(2)}$	0.240		
								$19a_{1\downarrow}^{(1)}$	0.075		
									147.04		

TABLE 7

	I.S. measured (in mm/s)	I.S. Predicted (in mm/s)
$Fe(CO)_5$	-0.174 ± 0.005	-0.174
$Fe(CO)_4$	- 0.124 ± 0.008	-0.06
$Fe(CO)_3$	-	+0.13
$Fe(CO)_2$	-	-0.04(C_{2V}) -0.38($D_{\infty h}$)
FeCO	-	-0.12

TABLE 8

	ΔEQ (in mm/s)		Calculated V_{zz} (in a.u.)	$\eta = \frac{V_{xx}-V_{yy}}{V_{zz}}$
	Calculated	Experimental		
$Fe(CO)_5$	+2.52	+2.52 ± 0.01	+1.57	-
$Fe(CO)_4$	+1.62	1.83 ± 0.02	+1.01	0.07
$Fe(CO)_3$	+1.08		+0.67	-
$Fe(CO)_2$ (C_{2v})	-8.02		-4.84	0.47
$Fe(CO)_2$($D_{\infty h}$)	-9.03		-5.64	-
FeCO	-5.77		-3.60	-

TABLE 9

$FeCO(C_{\infty v})$				$Fe(CO)_2(D_{\infty h})$			
Orbital	Energy (in eV)	Charge Distribution on Fe	One-Center V_{zz} per electron (in a.u.)	Orbital	Energy (in eV)	Charge Distribution on Fe	One-Center V_{zz} per electron (in a.u.)
$4\pi^2(\uparrow)$	- 6.12	91%($3d_{xz,yz}$)	- 1.246	$2\pi_g^2(\uparrow)$	- 7.41	83%($3d_{xz,yz}$)	- 1.107
$1\delta^1(\uparrow)$	- 5.77	100%($3d_{xy,x^2-y^2}$)	+ 2.765	$9\sigma_g^1(\uparrow)$	- 6.56	39%(4s) ,60%($3d_{z^2}$)	- 1.811
$11\sigma^1(\uparrow)$	- 5.65	31%(4s) ,66%($3d_{z^2}$)	- 2.014	$1\delta_g^2(\uparrow)$	- 6.48	100%($3d_{xy,x^2-y^2}$)	+ 2.764
$11\sigma^1(\downarrow)$	- 4.11	58%(4s) ,34%($3d_{z^2}$)	- 0.789	$2\pi_g^2(\downarrow)$	- 5.74	65%($3d_{xz,yz}$)	- 0.795
$4\pi^2(\downarrow)$	- 4.01	71%($3d_{xz,yz}$)	- 0.845	$9\sigma_g^1(\downarrow)$	- 4.92	41%(4s) ,56%($3d_{z^2}$)	- 1.323
$12\sigma^0(\uparrow)$	- 3.32	37%(4s) ,40%($4p_z$), 10%($3d_{z^2}$)	- 1.509	$1\delta_g^0(\downarrow)$	- 4.09	99%($3d_{xy,x^2-y^2}$)	+ 2.643
$1\delta^0(\downarrow)$	- 3.15	98%($3d_{xy,x^2-y^2}$)	+ 2.595	$4\pi_u^0(\downarrow)$	- 4.06	17%($4p_{x,y}$)	+ 0.404
$12\sigma^0(\downarrow)$	- 2.55	45%($4p_z$),42%($3d_{z^2}$)	- 2.256	$4\pi_u^0(\uparrow)$	- 4.06	23%($4p_{x,y}$)	+ 0.452

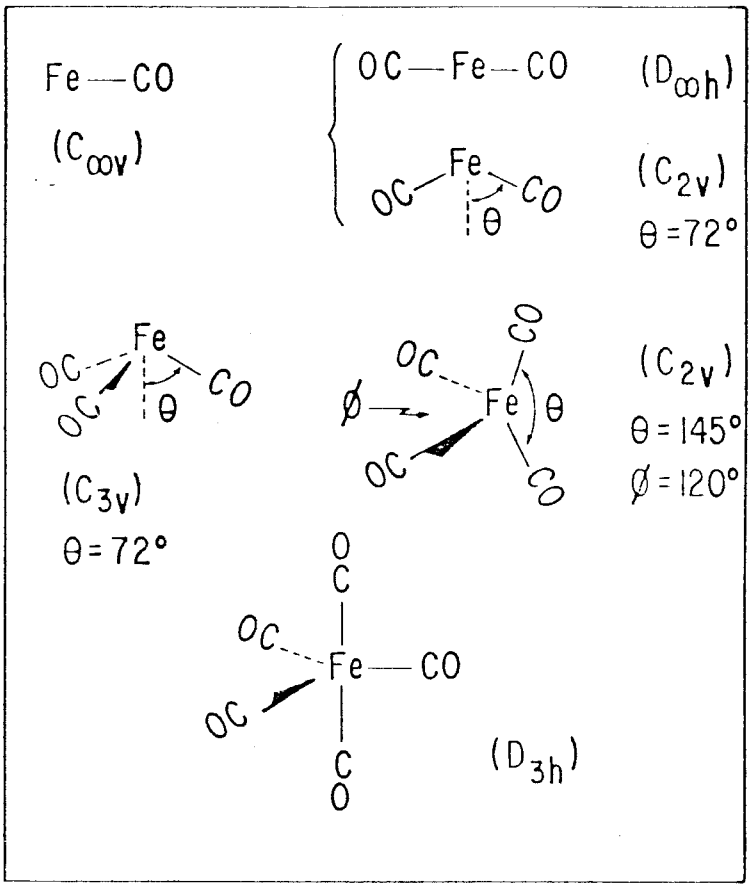
Fe—CO
(C∞v)
OC—Fe—CO
(D∞h)
Fe
OC
CO
θ
(C2v)
θ=72°
Fe
OC
OC
CO
θ
(C3v)
θ=72°
CO
OC
Fe
θ
Ø
OC
CO
(C2v)
θ=145°
Ø=120°
O
C
OC
Fe—CO
OC
C
O
(D3h)

FIG. 1

ENERGY (eV)
0
-10
-20
-30
Fe(4p)
Fe(4s)
C(2p)
Fe(3d)
O(2p)
C(2s)
O(2s)
2π
5σ
1π
4σ
3σ
1a'2
2e"2
6e'
5a"2
5e'
1e"2
9a'1
10a'1
7e'
6a"2
8a'1
4e'
4a"2
7a'1
6a'1
3e'
3a"2
5a'1
Fe(3d)
7e'
2e"
1a'2
6e'
1e"
10a'1
6a"2
5e'
5a"2
9a'1
8a'1
4a"2
4e'
7a'1
3e'
6a'1
3a"2
5a'1
2e"
8a"2
9e'
1a'2
11a'1
6a"2
6e'
10e'
3e"
7a"2
8e'
13a'1
7e'
1e"
12a'1
10a'1
5e'
9a'1
5a"2
8a'1
0
10
20
30
IONIZATION ENERGY (eV)
CO
(CO)5
D3h
(CO)5 + Fe
D3h
Fe(CO)5
D3h
Photoelectron
spectrum(a)

FIG. 2

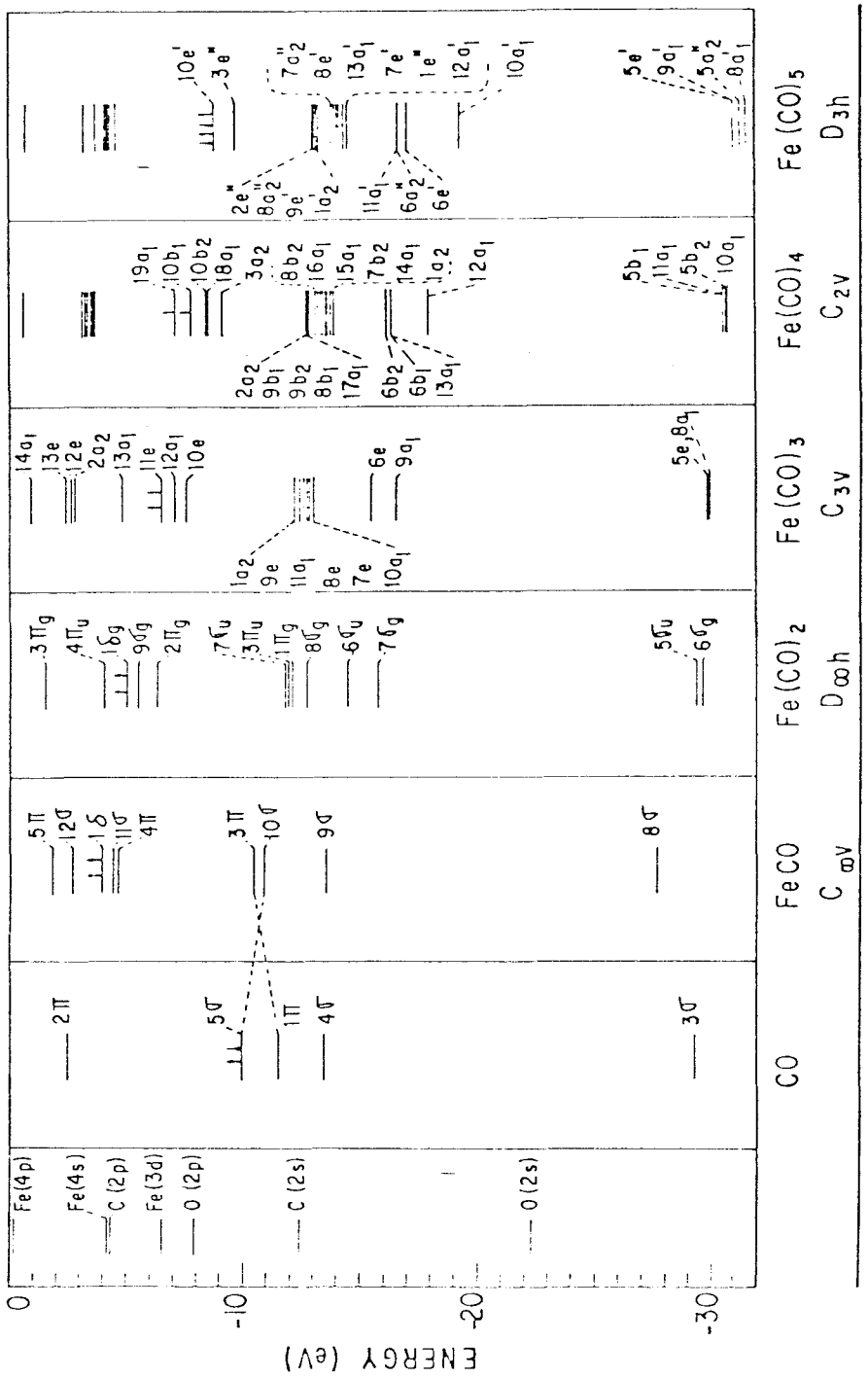
ENERGY (eV)
0
-10
-20
-30
Fe(4p)
Fe(4s)
C (2p)
Fe(3d)
O (2p)
C (2s)
O (2s)
CO
FeCO
Fe(CO)2
Fe(CO)3
Fe(CO)4
Fe(CO)5
C ∞v
D ∞h
C 3v
C 2v
D 3h

FIG. 3

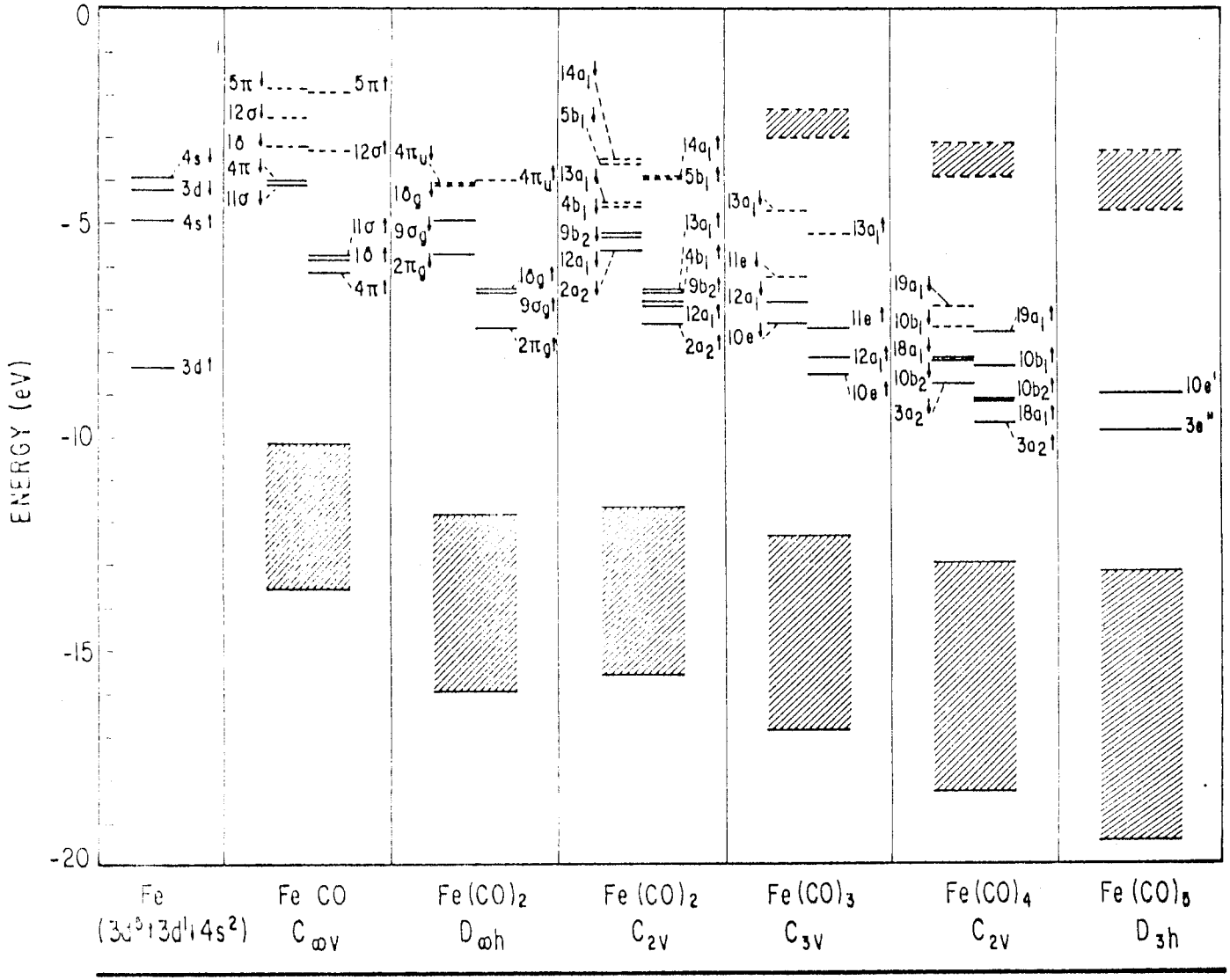
ENERGY (eV)
0
-5
-10
-15
-20
Fe
(3d⁶↑3d⁴↓4s²)
Fe CO
C∞v
Fe(CO)2
D∞h
Fe(CO)2
C2v
Fe(CO)3
C3v
Fe(CO)4
C2v
Fe(CO)5
D3h

FIG. 4